MAGNETORESISTANCE AND MAGNETO-THERMOELECTRIC TRANSPORT IN A THIN COBALT FILM ON HEXAGONAL BORON NITRIDE AND SILICON DIOXIDE SUBSTRATES

Department of Physics and Astronomy

The University of Manchester

Semester 1 Mphys report

December 2018

Ben Snow

9630490

Abstract

Ferromagnetic materials, such as cobalt, play a large role in modern electronic storage devices and the downsizing of such devices brings about new problems[1]. As such, a device was designed and fabricated to test the electrical and thermal properties of a thin cobalt film on two substrates: hexagonal boron nitride and silicon dioxide. Gold contacts placed on the channel allowed the resistivity of this channel on silicon dioxide to be measured to be $(26.75 \pm 0.27_{\text{Random}} \pm 0.71_{\text{systematic}})\mu\Omega m$ which is consistent with other films of this nature on similar substrates. Anisotropic magnetoresistance in the channel was also found to be consistent with literature. A fabricated gold heater was used to create a thermal gradient along the channel and as such, the thermopower was measured to be $(-16.7 \pm 3.3_{\text{Random}} \pm 2.1_{\text{systematic}})\mu V/K$ on the SiO_2 which is similar to that reported by Avery et al[2] for a similar cobalt film. The variation of this thermopower with magnetisation direction of the film was too consistent with literature. Unfortunately, no measurements on the hBN substrate could be made due to mistakes in the fabrication process but this leaves room for further study next semester after repairing the device. A test of the thermal profile along the channel revealed that the temperature gradient is largely unaffected by the direction of the magnetisation of the channel.

Contents

Introduction

As the need for the storage of large amounts of data increases, better and higher capacity storage devices are needed. This leads to the miniaturisation of current magnetic storage devices to increase their capacity and improve storage efficiency. As these devices get smaller, heat can start to affect their operation. Ferromagnetic thin films are a common building block in magnetic storage and, as such, it is important to study the physics surrounding heat transport and in particular magneto-thermoelectric transport in these thin films. The end goal of research in this field is to make these devices more efficient and waste as little heat as possible during their operation.

Thermal transport in thin films is a field is closely linked to spintronics: an area of research that concerns the drift and diffusion of spin through electrically conducting materials. New technologies such as Magnetic Random Access Memory and Giant Magneto Resistance rely on the flow of spin in conductors and the effect that magnetisation has on this flow[3]. Spintronic devices consist of a thin ferromagnetic material known as a channel with thicknesses of the order of 10-100nm. One popular metal used as a channel is cobalt due to its ferromagnetic nature and high electrical conductance. Attached to this channel are metallic contacts that can be used to inject charge or spin currents into the channel and also to measure potential differences, temperatures or spin accumulation. Channels like this are typically grown through lithographic techniques, discussed later in the fabrication section, on substrates such as silicon dioxide and hexagonal boron nitride (referred to as 'hBN' from now on). Depending on the properties of the substrate on which the channel resides, transport of charge and spin through the channel can be greatly affected.

It is not yet known how thermal transport occurs through thin cobalt films on hBN substrates. It is thought that hBN may enhance the thermal properties of the cobalt channel, due to its high thermal conductivity. Current research has been conducted on thermal and electronic transport in thin cobalt films on SiO_2 substrates.[2], [4]–[6] Anisotropic magnetoresistance and magnetothermopower, discussed in detail later, in these devices have been measured and can be compared to what is measured in this paper. A comparison can then be drawn on the effect of the hBN substrate compared to the SiO_2.

Magnetisation and resistivity

Materials are made up of many atoms composed of a nucleus and electrons. Electrons orbiting this nucleus act like a current flowing in a circle. Orbital angular momentum gives rise to a small orbital magnetic moment that points in the direction perpendicular to the plane of the orbit. Orbital magnetic moments are quantified by $\boldsymbol{\mu} = -\mu_B \boldsymbol{L}$ where μ_B is the Bohr magneton and $\boldsymbol{L}$ is the orbital angular momentum. An even larger contribution to the magnetic moment of an atom comes from the electron spin and it is quantified by $\boldsymbol{\mu} = -g\mu_B \boldsymbol{S}$ with g being the Lande g factor (2 for electrons[7]) and $\boldsymbol{S}$, the spin angular momentum. These electrons therefore act as little bar magnets producing their own small magnetic field. These tiny bar magnets can be oriented in different directions with an externally applied magnetic field. Magnetisation of a material is defined as the sum of the magnetic moments $\boldsymbol{\mu}_n$ of the atoms in a volume V divided by the volume of that material: $\boldsymbol{M} = \frac{\sum_n \boldsymbol{\mu}_n}{V}$. When more and more spins are aligned, the overall effect of magnetisation arises. An externally applied magnetic field, $\boldsymbol{H}$, can be used to change the direction of this magnetisation vector as it creates a torque $\boldsymbol{\tau}$, on the magnetic moment leading to a rotation, $\boldsymbol{\tau} = \boldsymbol{\mu} \times \boldsymbol{H}$. Magnetic moments align with the direction of $\boldsymbol{H}$.[7]

Exchange energy, E_{ex}, can be used to understand why neighbouring spins tend to align in the same direction. Electrons in close vicinity to one another have overlapping wave functions and, as

such, are subject to the Pauli Exclusion Principle. The energy needed to exchange two neighbouring electron spins expressed mathematically as $E_{ex} = -2JS_1S_2cos\theta$ where J is the exchange integral coming from the overlap of the wavefunctions of the electrons, S_{12} are the spins of the electrons and θ is the angle between the directions of the two spins. E_{ex} is minimised if θ is zero degrees, parallel alignment, and is maximised for $\theta = 180^O$or antiparallel alignment. Therefore spins next to one another will tend to align themselves to the direction of their neighbours, this is the origin of ferromagnetism. The shape of a material then can affect the magnetisation direction. It may be easier to point the magnetisation direction in one direction as opposed to another. This leads to the idea of an easy or hard axis. This idea is exploited in nanodevices to make the easy axis as easy to magnetise along as possible by restricting the dimensions of a material in all other direction. A very long thin wire of cobalt, for example, would have a very easy axis along its length but very hard axes along the width and depth. A visual representation of easy and hard axes can be seen in Fig.1.

Changing the direction of magnetisation in a conductor was discovered to change the resistance of a conductor by up to 5% [8]. This effect is known as anisotropic magnetoresistance and figure 2 shows an easy was of visualising this. In essence, the resistance of the material is increased when the magnetisation points in the same direction as the current. Electron orbitals can be thought of as semi solid disks that can be rotated from being upright to being flat. The magnetisation direction of the material is perpendicular to the surface of these disks. An upright disk related to magnetisation and current direction being parallel to one another and a flat disk when current is perpendicular to magnetisation. For incident electrons attempting to pass through the material, it is easier to pass through the flat disks than the upright ones due to the decreased scattering area so the resistance of the material is lower for perpendicular magnetisation and current directions. The opposite is true for the parallel orientation of the current and magnetisation. Unlike resistance, the resistivity, ρ, of a material is intrinsic to it. Resistance may change with the size and shape of a material but the resistivity remains constant. Resistance, R, therefore can be measured and converted to resistivity for comparison with literature by use of the dimensions of the material in the formula $R = \frac{\rho l}{A}$. Here l is the length along which the current passes and A is the area that the current passes through. To quantify the change in resistivity due to magnetisation direction changing a percentage change in resistivity is calculated. $\%AMR = \frac{\rho_{||} - \rho_{\perp}}{\rho_{||}} * 100$ [4]where $\rho_{\perp}$ is the resistivity of the channel measured when the magnetisation is perpendicular to the current direction and $\rho_{||}$ is the resistivity measured when magnetisation and current are parallel. Resistivity of a

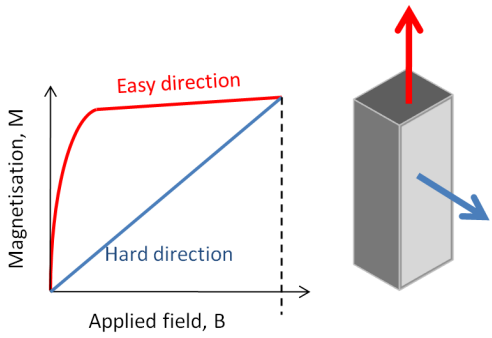

Figure 1: A very small external magnetic field is required to rapidly increase magnetisation along the easy magnetisation direction. Magnetisation can be forced to point in the hard axis direction but a much higher external field is needed to do so.

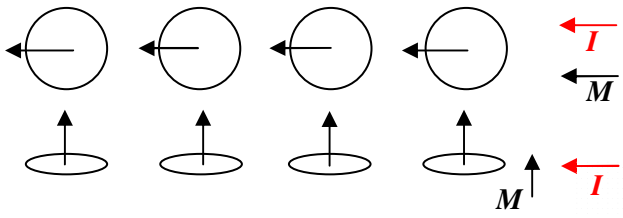

Figure 2: For magnetisation, *M*, pointing in the same direction as current, *I*, the apparent scattering area of the orbitals is larger so the resistance in this orientation is high. When *M* and *I* are perpendicular this scattering area is reduced and so resistance also reduces.

ferromagnetic material depends on the angle between the applied magnetic field and the direction of current through it by the following relation $\rho(\varphi) = \rho_{\perp} + (\rho_{||} - \rho_{\perp})\cos^2\varphi$ [9] where φ is the angle between the current direction and the magnetisation. By applying a magnetic field to the channel and increasing its magnitude, the magnetisation direction can be rotated therefore varying φ. This is the principle on which AMR was measured in these experiments.

Thermoelectrics

One effect that occurs in thermoelectrics is called the Seebeck effect, also known as longitudinal thermopower. This is the effect whereby heat is converted into electricity was discovered in 1774 by Alessandro Volta.[7] In essence, a temperature difference across a conductor causes negative charges, electrons, to flow in the conductor from the hot area to the cold area. The ratio of the potential voltage, ΔV, that arises due to a temperature difference, ΔT, is known as the 'Seebeck coefficient or the thermopower: $S = -\frac{\Delta V}{\Delta T}$. Quoted values of seebeck coefficient are typically given relative to the contacts used to measure it, all measured seebeck coefficients are in reference to gold in this paper. Thermopower is intricately linked to the resistivity of a material and the applied magnetic field to that material via the 'Mott relation'

$$S(E) = -\frac{\pi^2}{3}\frac{k_b T}{e}\frac{1}{\rho(E)}\left[\frac{\partial\rho(E)}{\partial E}\right]_{E=E_F} \tag{1.1}$$

here k_b is the Boltzmann constant, T is the temperature of the conductor, e is the charge on a charge carrier moving through the conductor (1 unit of electron charge here), ρ is the resistivity of the conductor and E_F is the Fermi energy of the conductor.[10] It is evident, therefore, that the sample magnetisation direction and the current direction due to the response of resistivity to magnetisation direction of the channel, the seebeck coefficient should change with magnetisation direction too. A figure of merit used to quantify the size of this effect is the MagnetoThermoEletricPower, MTEP, and it is defined as such: $MTEP = \frac{S_{||} - S_{\perp}}{S_{||}} * 100$ where $S_{||}$ and $S_{\perp}$ are the seebeck coefficients measured when the thermal gradient is parallel and perpendicular to the magnetisation direction.

Design considerations

An important part of the research to be conducted in this project concerns the effect of magnetisation direction of a thin cobalt film on the thermoelectric transport through the film. This phenomenon will be studied in a 30nm thick cobalt film two different substrates: Silicon Dioxide (SiO_2) and Hexagonal Boron Nitride (hBN). SiO_2 can be easily produced by oxidising the top layer of a pure silicon wafer through a procedure known as LOCOS (LOCal Oxidation of Silicon)[11], in order to create an electrical and thermally insulated platform on which solid state devices can be built. SiO_2 has been the dominant substrate of choice for integrated circuits and microdevices since the 1960s due to its chemical stability and excellent electrical and thermal insulation properties. hBN, on the other hand, is one of the best electrically insulating, thermal conductors there is, and it is also atomically flat unlike SiO_2 that has high surface roughness.[12] The difference in flatness between hBN and SiO_2 will cause the cobalt to grow differently giving rise to different slightly different crystalline structures in the cobalt. This effect will be quantified in the difference in magntoresistive measurements on SiO_2 and on hBN.

In order to see how the magnetisation direction of a thin film affects the magnetoresistance of the material, a suitable metal must be used to build the film. Cobalt was chosen to be used as the channel due to its ferromagnetic nature and high thermal and electrical conductivities. Cobalt is used

in the study of many spintronic devices[4], [13]–[15] as it can be reliably evaporated and deposited onto substrates which will be discussed in more detail in the 'Fabrication' section of this paper.

To isolate thin flakes of hBN the method, used originally for the isolation of single layer graphene by Geim and Novoselov of exfoliation is used. [16] This method uses adhesive tape to peel off layers of hBN until there are only a few layers left. These flakes of hBN are then transferred to a pre-prepared wafer of SiO_2. Flakes of hBN can then be found and characterised with the use of an optical microscope. Figure 3 shows an optical image of the hBN flake used in this experiment.

hBN flakes are required to be as thin as possible as the thermal conductivity increases as the number of hBN layers decreases. In my experiment I want to use a material with a high thermal conductivity to magnify the thermal profile through the cobalt channel. Measured MTEP versus the SiO_2 may be larger due to heat flowing through the hBN flake underneath and into the channel as opposed to on the thermally insulating SiO_2. Flakes also have to be as thin and flat as possible since there cannot be a large discontinuous boundary between the hBN edge and the SiO_2 beneath. Only a small amount of cobalt (30nm) is being deposited on to the substrates so if the flake is too thick, then the cobalt channel will not be connected over the hBN/SiO_2 interface.

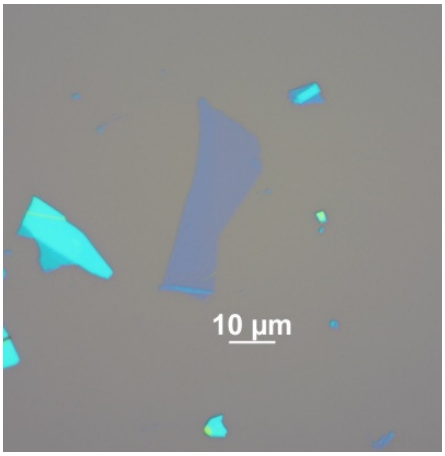

Figure 3: The optical image above shows a dark blue flake of hBN of thickness approximately 6nm, measured from AFM imagery. It is of order 10µm wide which is sufficient to hold a cobalt channel and possibly a heating element. SiO_2 can be seen as the grey background and surrounding the dark blue flake are thicker light blue flakes of hBN and other impurities.

A flake was selected with approximate thickness of 6nm and width of around 10µm. This flake appeared to have few folds or discontinuities and was large enough to hold half of a 20µm long cobalt channel. This flake rests on a grey SiO_2 background and is surrounded by other flakes of hBN of different thicknesses. Light blue flakes seen in Fig 3. are thicker than the dark blue flake that we are interested in. Care is needed to avoid deposition onto surrounding flakes in later stages of fabrication as they may cause discontinuities in contact wires leading to unusable contacts.

After the flake of hBN was selected, an electrical contact pattern was designed. Here the steps taken that lead to the final design, seen in figure 4, are discussed in detail. Firstly a cobalt channel, the central light blue rectangle in figure 4b) and c), was required, this was to be situated on both the hBN and SiO_2. The channel had to be thin and narrow to form an obvious easy axis along which, the magnetisation would naturally lie. Magnetisation can then be rotated through the 2nd easiest axis (XY direction as labelled in figure 4c) by application of a magnetic field. For the flake chosen, a cobalt channel with a length of 17µm and a width of 2µm was chosen. Its thickness is 30nm, nearly 100 times smaller than the next axis length to again exaggerate the shape anisotropy of the channel.

Photos of the sample were taken at different levels of magnification and then imported into a software package called LayoutEditor. This is specialised software used to design nanoscale structures that are created through Electron Beam Lithography. Lines and shapes were drawn on top of the optical images of the flake candidate that were then used by the operator of the EBL machine to fabricate the design.

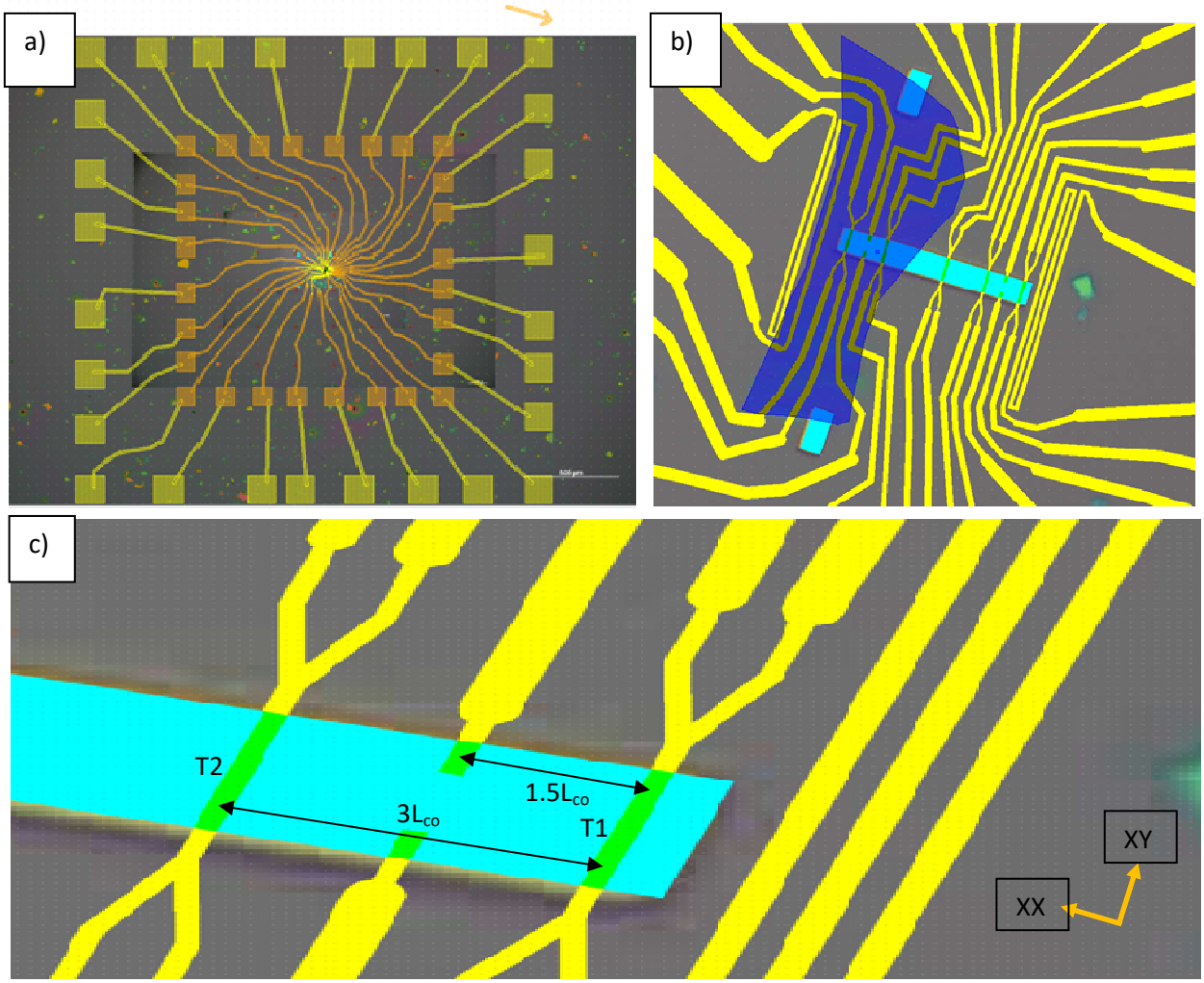

Figure 4. These computer generated images show the finalised design sketches drawn up in Layout Editor ready for use in the lithographic stage of fabrication. a) The entire design. Yellow and orange squares are inner and outer bonding pads and they measure 100μm and 150μm across, respectively. Gold wires were drawn from the bonding pads toward the device which is situated in the centre of the image. The orange arrow in the top right of a) is positioned parallel with the cobalt channel and is used to align the wafer on the chip carrier. b) Shows the hBN flake as dark blue with the overlaid contact design in yellow and the cobalt channel (horizontal rectangle) and two anchors in light blue. c) shows a close-up of a section of the device labelled with dimensions and distances between thermometers T1 and T2.

Anchors of cobalt, seen as the light blue rectangles at the top and bottom of the main dark blue flake, were designed to be deposited on the edges of the hBN flake. It was hoped that the anchors would limit movement during transport of the device between different lithographic steps (described in the 'Fabrication' section). Quite the contrary ended up happening and one of the anchors came loose and destroyed part of the upper left hand side of the device.

To measure the resistivity of the cobalt channel and in turn quantify AMR in the channel, a series of electrical contact s were needed to be placed along the length of the channel. These contacts, seen as yellow or orange in figures 4 a, b and c, were designed to be made from gold, a highly conducting metal with a low thermopower. Low thermopower is useful as it will not greatly increase measured thermopower of the cobalt channel. Thermometers were designed to have four leads

attached to them so that a four terminal measurement technique could be implemented. Four terminal measurements eliminate lead resistances to the contacts and thus give a more accurate reading.

A thermal gradient through the channel can be produced by fabricated heaters that work on the principle of Ohmic heating. Heaters are situated at each end of the cobalt channel, one positioned on the SiO_2 and one partially situated on the hBN. Electrons moving through a conductor collide with ions and are scattered giving rise to heat generation. The power of heat outputted by a heater, P, is proportional to the square of the current, I, passing through it multiplied by the resistance of the heater, R, related by the following equation $P \propto I^2R$. Therefore, to achieve a large thermal gradient, it is useful to use a high current through the heater being careful not to use too much as the heater may be overloaded and could break due to its small size. It is useful to use a large snake patterned heater with multiple bends to increase the overall resistance of the heater. Heaters must be sufficiently wide compared to the width of the channel to provide a homogeneous thermal gradient throughout the channel. A homogeneous thermal gradient will reduce any 'current bunching' in the channel. Hot spots and cool spots will cause a non uniform current flow through the channel. Designed heaters are 20μm in width approximately 10 times the width of the channel.

To quantify this thermal gradient, five gold thermometers were placed along the length of the cobalt channel. T1 was placed at the edge of the channel, to measure the temperature as close to the heater as possible. T2 was then placed far enough away from T1 to allow for a measurable difference in temperature in the cobalt channel. This distance is approximately three times the characteristic thermal length in cobalt $L_{co} = \sqrt{\frac{\kappa_{co} t_{SiO_2} t_{co}}{\kappa_{SiO_2}}} \approx 1.1\mu m$ where κ_{co} and κ_{SiO_2} are the thermal conductivities of cobalt $140 W/mK$[2] and SiO_2 $1 W/mK$[17]. t_{co} and t_{SiO_2} are the thicknesses of cobalt, 30nm, and SiO_2, 300nm[17]. A measureable temperature difference is required so a separation of $3L_{co}$ between thermometers was used. This is analogous to assuming a capacitor is fully charged after three time periods of charging.

Hall bar architecture was added to the device in order to measure transverse magnetoresistance and to measure the planar Nernst effect (or transversal thermopower). Unfortunately, due to issues with fabrication, only one hall bar was left intact so no hall bar measurements could be made. In the future, these could be re-patched and used for further measurements. All thermometers and hall bars are of width 200nm and the heater wires are 300nm wide, all contacts were made by depositing 40nm of gold and 3nm of chromium. Wires get thicker, up to 10μm in width, the father out from the device they are to increase robustness and reduce chance of breakage or, in the case of the heater, unwanted additional heating.

Tolerances within the design

The fabrication process involves several stages, all of which have limitations and so my design was built to a certain tolerance level to account for this. hBN flakes are held in place on the SiO_2 by the weak van der Waals force so are liable to move around slightly between lithographic processes. The cobalt anchors were put in place to reduce this movement but a tolerance of 500nm of movement between designed contacts and the hBN flake was used. The electron beam has a non zero width and so a gap of at least 300nm between any contacts was used to limit overlap and shorting between contacts.

Fabrication

Lithographic process

After design was finished it was time to make the device. Similar devices to mine have been produced in the past with a high level of success. Fabrication is a complicated process and requires training with equipment that I did not have experience with. Instead, fabrication was performed by two PhD students, Victor Guarochico Moreira and Noel Natera Cordero, who have much experience. As discussed previously, the device will be fabricated on top of a flake of hBN resting on a silicon dioxide capped wafer of silicon. The whole process begins with a large, pre-prepared, high purity silicon wafer. A tool called a scriber is then used to cut out a square a few cm in width. As stated in the design stage, the hBN flake, isolated through the exfoliation method[16] was placed onto the silicon square. It was at this point that the initial optical images of the flake were taken seen in figures 3 and 4.

Electron Beam Lithography (EBL) began by uniformly covering the wafer with polymethylmethacrylate (PMMA) in a process known as spincoating. Spincoating involves placing a small amount of PMMA on the centre of the sample then rotating it at speed to evenly spread out the material. PMMA is a photoresistive polymer that contains long chain molecules that can be broken under exposure to an electron beam. Broken molecules can be washed away with a solvent whereas the unexposed PMMA remains unaffected. After exposure, the sample is taken out of the EBL chamber, inverted, and placed on the ceiling of an evaporation chamber. Here, a small pellet of gold or cobalt, for example, is placed underneath the sample. An electron gun is then fired at this pellet causing it to evaporate and then move towards the top of the chamber. This evaporated gold covers the whole sample covering the PMMA and the holes left in the PMMA. Evaporation lasts for a set amount of time to deposit a known thickness. Another solvent is used to wash away the residual PMMA and gold (for example) leaving behind only gold left in the shape cut out by the electron beam.

For fabrication of my device, firstly the chip had to first be properly aligned to the EBL viewfinder. To do this a set of uniformly distributed crosses were drawn and deposited with gold. Photographs of the chip were then taken and design drawings in Layout Editor were scaled and aligned to these crosses. The next deposition onto my device was the cobalt channel and anchors and the gold capping layer on top of them. A 3nm capping layer of gold was deposited on top of the cobalt channel to stop oxidisation between the cobalt and chromium gold deposition processes. A few issues arose during this first deposition that will be talked about in the next section.

Finally, the 3nm chromium and 40nm gold contacts were deposited on top of the cobalt channel by the same process. Continuity checks were made between each of the contacts present on the channel to make sure that they are connected correctly. It was found that four contacts were found to be open circuit (not connected to the device), these included the hBN heater and the leftmost thermometer in figure 4c. Two other contacts were accidentally electrically connected due to an issue with the viewfinder.

Accidents and mistakes during fabrication

Several issues occurred during the fabrication process that caused large setbacks in achieving the initial goal outcomes of the project. Firstly, during the cobalt deposition, ‘ears’ formed at the end of one end of the channel due to a tear in the PMMA. These ears can be seen in the AFM (atomic force microscopy) image in Figure 5 as two lines erupting from the corners of the rectangular channel

caused by overfilling of the resist with cobalt. This tear meant that additional cobalt ended up being deposited on the hBN. This effect is documented to have happened in the past. [18]

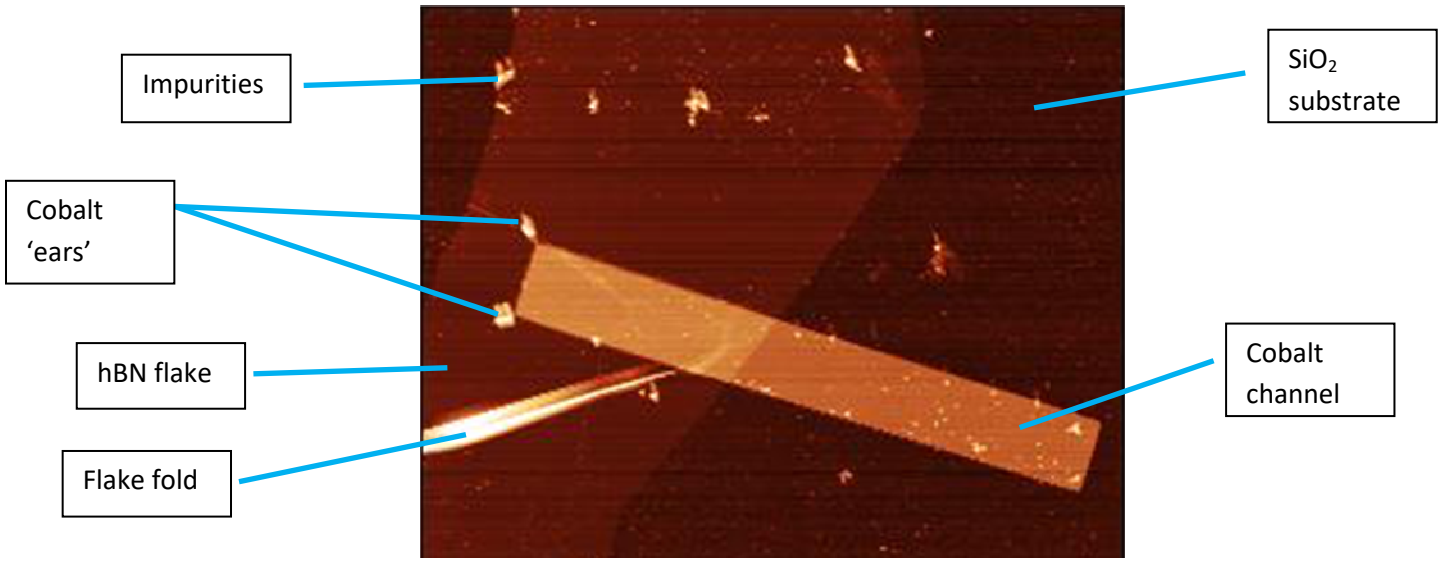

Figure 5. This false colour AFM image shows the rectangular cobalt channel resting on top of the hBN and SiO_2 substrates. A large fold in the hBN flake can be seen in the bottom left hand side of the picture.

After the deposition of the cobalt channel, a fold had appeared on the hBN in the bottom left quarter as seen in figure 5. Analysis conducted in AFM software analyser, Gwyddion (http://gwyddion.net/), revealed that the fold was of the order of 100nm in height, one micrometer in width and extended seven micrometers across the flake. Other researchers in my group had experienced this issue with hBN before and they found that depositing at least 30nm of gold over the discontinuity would be substantial enough to maintain good electrical contact. After deposition it was found that the contacts deposited over this fold were open circuit.

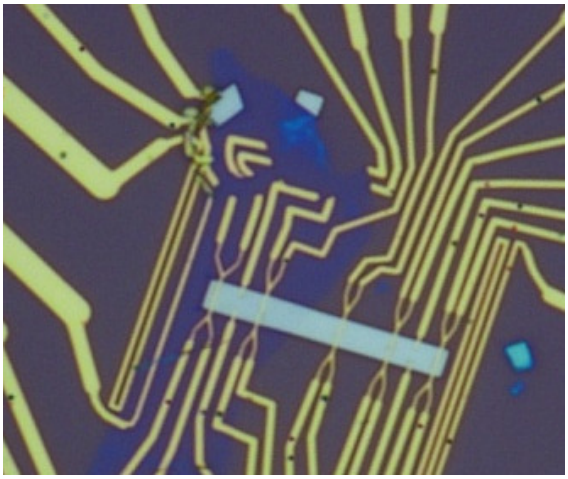

Figure 6. Here the broken flake and cobalt anchor can be seen in the top left quarter of the image. Only 4 contacts on the hBN remained intact but no thermometers were of use.

Cobalt anchors used to hold the flake in place may have caused the hBN flake to fold over and cause a large break in many of the contacts. This was a major setback for the project as there were no functioning thermometers on the hBN sample. This collapse can be seen in figure 6 to the left. Instead of focussing on comparing thermal measurements on and off the hBN substrate, the goal shifted to measuring electrical and thermal transport only on the SiO_2. Next semester there will be attempts made to patch the broken contacts with another gold deposition.

Mounting the device

After device fabrication the silicon wafer was cut down to a square small enough to fit onto a 3mmx3mm chip carrier. This cutting down was performed with a scriber, a device that makes a precise, straight line cut along the silicon's surface, the wafer is then broken along this line to leave a clean cut. The wafer was cut down to have dimensions of 2.5mmx2.5mm. Next, the chip was mounted into an LCC, a leadless chip carrier, by sticking it down with silver paint. Here the wafer is aligned with the arrow in the top right corner of the design that is parallel with the channel direction. This makes sure that the channel is oriented horizontally in the chip carrier. After this, a wire bonding machine was used to solder the outer contacts on the fabricated device to the LCC contacts. Only 20 of the 28 contacts on the device were soldered to the LCC since 8 were found to be open circuit by continuity checks performed after fabrication.

Experimental procedure

To experimentally measure the AMR and thermoelectric responses of the cobalt channel a sophisticated experimental setup was needed. The device, mounted in the chip carrier is carful placed and secured at the end of a cryostat (Oxford Instruments® Microstat HE2). This then connects through a series of wires to a breakout box which has 24 twist lock sockets, each linking to the 24 contact pads on the device. From here, electrical measurement apparatus can be connected to inject current into the device or measure voltages for example. The cryostat has a radiation shield around it to limit external interference. A turbo vacuum pump was also attached to the cryostat that allowed for quick pumping of the system to 10^{-6} barr. A thermometer/global heater with a PID controlled were attached to the cryostat also and were used to measure the temperature of the device and keep the entire setup at a constant temperature. The cryostat itself was then mounted between two magnetic coils which are attached to a cooler. All of these pieces of equipment can be seen in figure 8.

Minute changes in voltage are required to be detected so specialised equipment will be used. A lock in amplifier, see figure 8, is very useful for detecting signals that would be undetectable due to noise in a system. It works on the simple principle of orthogonality of the sine functions. A reference sinusoidal signal, $sin(\omega t)$, is generated inside the lock in amplifier at a frequency ω, this is then multiplied with the input signal, $A(t)$.The input, $A(t)$, is the sum of many sine waves including the signal that we wish to measure. When the product of $sin(\omega t)$ and $A(t)$ are integrated over a time period T the orthogonality of the sine functions gives zero for all sine waves not at frequency ω thereby eliminating a vast array of noise. This gives a D.C. output whose amplitude is the half the limit of this integral when T goes to infinity. Expressed mathematically, the output D.C. signal is $A_{out}(t) = \frac{1}{T}\int_{t-T}^{t} \sin(\omega t)\, A(t)\, dt = \frac{1}{2} V_{sig} cos(\theta)$ where V_{sig} is the signal amplitude and θ is a phase difference between the signal and reference that is adjusted to give the maximum output signal.[19]

To eliminate lead resistance, a four point measurement technique was used. An example circuit diagram of a four point resistance measurement can be seen in figure 7. Resistance is only measured through the overlap of current injection and voltage measurement therefore eliminating the lead resistance

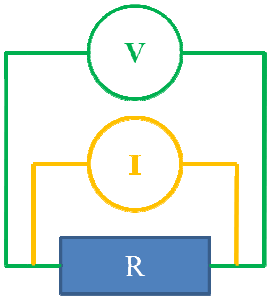

Figure 7: On the right a four point measurement technique is shown. Here the potential difference (green) is measured across the resistor, *R*, where the current, *I*, (orange) is present.

Figure 8. a) breakout box with 24 twist lock sockets b) centre is the lock in amplifier and beneath is the temperature controller and PID c) Kiethley variable source meter d) magnet coils and mount for cryostat e) SR560 preamplifier f) variable series resistor

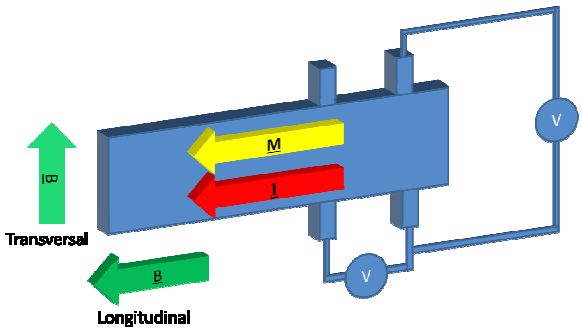

Figure 9: Potential difference across the length and width of the channel can be seen here. The magnetisation $\underline{M}$ of the channel can be rotated by a transversal or longitudinally applied magnetic field, $\underline{B}$. Current $\underline{I}$ is perpendicular or parallel to the applied magnetic field direction.

Voltage measurements were taken across the width of the channel and along its length. Applied magnetic field was either varied longitudinally or transversally as seen in figure 9. Magnetisation direction $\underline{M}$, was rotated by an external magnetic field $\underline{B}$. Current $\underline{I}$ was present in the channel. For thermal measurements, the fabricated heater (not pictured in figure 9) was connected to a series resistor of $1k\Omega$, figure 8 f). This was done as a safety precaution to limit the maximum current through the heater to $5mA$ when the potential across the heater and series resistor was $5V$.

Results

Thermal calibration

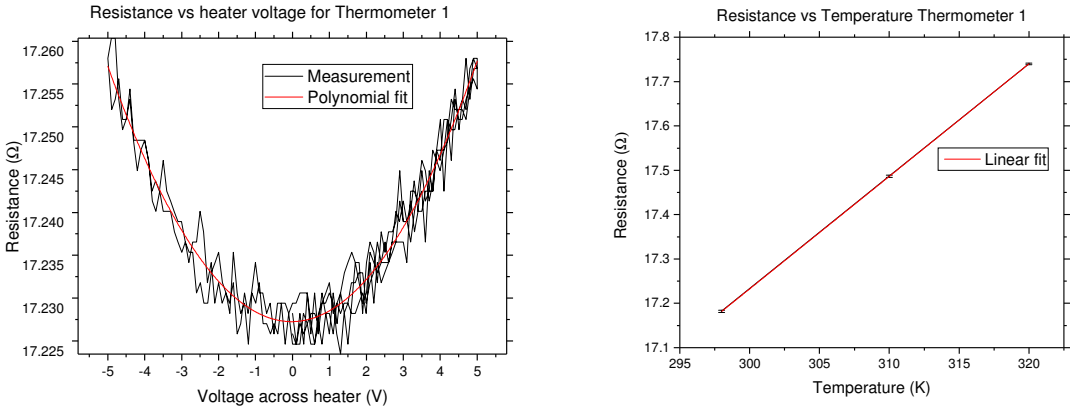

Figure 10. a) Resistance of thermometer 1 for a given potential difference across the heater. b) Resistance of T1 as a response to global temperature increase.

A relationship between the heater voltage applied and the resistance of a thermometer on the channel was first needed to be found before any thermopower measurements could be taken. This response is expected to be quadratic since a change a resistance is proportional to the temperature difference caused by the heater.[20] This temperature difference is related to the power emitted by the heater which is quadratically related to the voltage applied to the heater:

$(R - R_0)\ \alpha\ (T - T_0)\ \alpha\ P\ \alpha\ {V^2}_H$. Where R and T are the thermometer resistance and temperature measured with an applied heater voltage V_H and R_0 and T_0 are the resistance and temperature measured when $V_H = 0$. P is the power dissipated by the heater. Therefore we can say that

$R = \beta\ {V^2}_H + c$. The quantity β can be extracted with a fitting error from fitting a quadratic curve to measured data, shown in figure 10 a. Since we are only interested in the shape of the curve and not the offset from zero we can ignore c. The hBN thermometer did not yield sensible results and can't be used as an accurate thermometer due to 3 point measurement being used.

Next the global heater was used to warm up the entire sample. This gave a relationship between global temperature of the thermometers and their resistance seen in figure 10 b). It is easy to then calculate the temperature difference, ΔT, in the cobalt channel by taking the difference in the change in temperature between two thermometers. Now it was assumed that this ΔT is constant for a given heater voltage, since the effect of magnetisation direction is unknown. Table outlines the α values and β values and their respected uncertainties. All that was needed now was the voltage drop between two thermometers and the ratio of this to ΔT gave the thermopower, S.

Longitudinally varying magnetic field

The next important set of experiments concerned determining the resistivity and AMR of the cobalt channel on and off the hBN substrate. Unfortunately due to the problems in fabrication neither of the thermometers on the hBN were fully operational so temperature and voltage measurements could only be made on the SiO_2.

Since AMR is such a small effect, on the order of 0.4% for film of this nature[4], random noise can be an issue when trying to measure it. As a result, the magnetic field was swept many times (of order 40) to obtain as many repeat measurements as possible as well as noise reduction from the lock in technique. Repeated measurements were then spliced up into traces and retraces by an Origin script (see appendix). The traces contain data taken when the current applied to the magnetic coils varied from negative to positive, denoted by black lines on Figure 11. Contrary to this, the retraces contain data of positive to negative applied current. Averaging, carried out by the same script, was then performed to produce the average AMR curves shown as the bold lines in a) and b). These initial averages took into account all of the trace (or retrace) data. The minimum point of different traces (retraces) differed from the true minimum resistance value because the channel may not have been fully saturated at high magnetic field. Reversal of the magnetisation direction, in this case, would then be easier and a lower magnetic field would be required to rotate the magnetisation vector through the hard axis to the opposite easy axis. Since measurements are taken while at temperatures of near 300K, thermal fluctuations could have also caused the magnetisation vector to rotate differently.

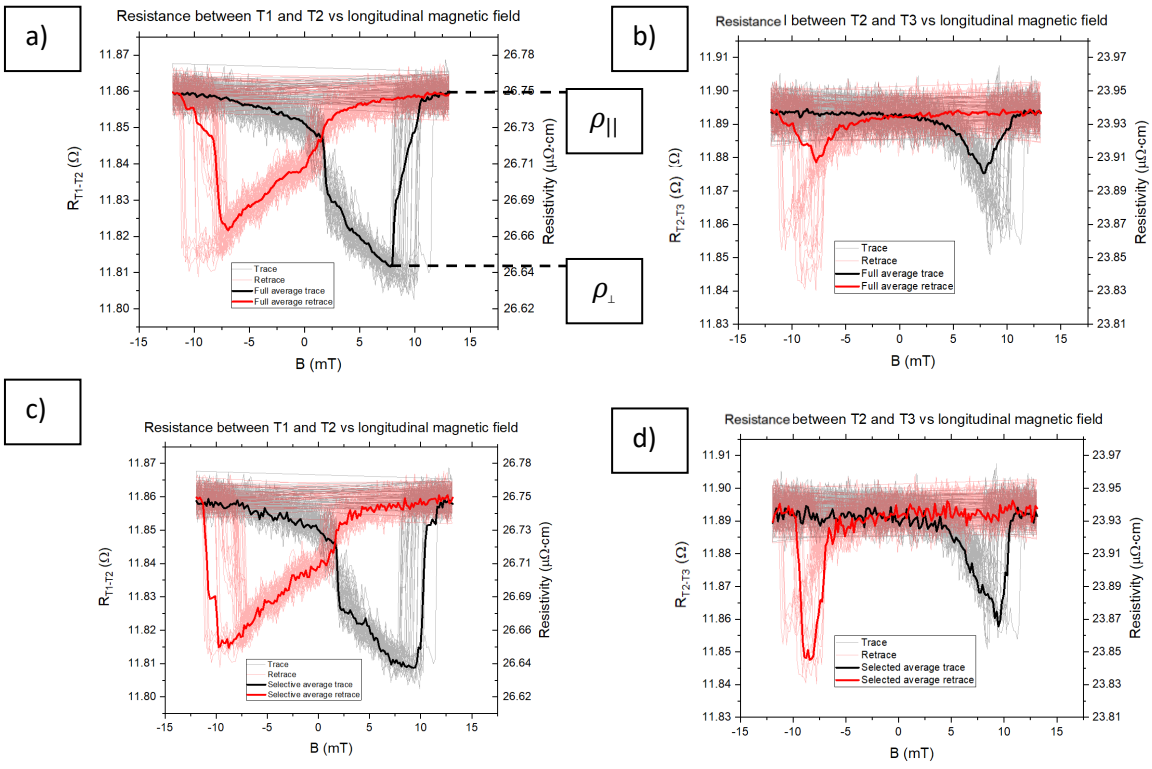

Figure 11. Magnetic field dependent resistance of the channel between two consecutive thermometers. a) and c) show the resistance of the channel between T1 and T2 (as labelled in figure 4) and b) and d) show the resistance of the channel between T2 and T3. The right hand side axis shows the resistivity of the channel as calculated from the dimensions of the cobalt between pairs of thermometers. The magnetic field is varied parallel to the direction of current injected into the channel.

When all trace (retrace) data is used in the averaging algorithm, the minimum resistance value produced is skewed to a higher, non physical value since more data appears in the data set with high resistivity than at low resistivity. This is most notably seen in figure 11 b). Averages produced this way have very high precision but low accuracy and lead to an overestimation in the minimum resistivity value and an underestimation of the percentage AMR observed. To negate this effect, a select few curves with the lowest minima were used to calculate a separate average, these averages can be seen as the bold lines in figure 11 c) and d) This average is slightly less precise than that of the full average due to the lower signal to noise ratio but the minimum value of resistance produced is more accurate to the true value.

Resistivity of the channel

Before discussing the AMR effect in the cobalt channel, it is important to first look at the c resistivity and check that it is consistent with previous experimental literature. To do this, the following formula to calculate resistivity was used: $\rho = \frac{V}{10I}\frac{wt}{l}$ where V is the voltage measured between contacts, I is the known current through the channel, w is the width of the channel, t is the thickness of the channel and l is the separation of the contacts, the factor of 10 comes from the pre amplifier. For the longitudinally varying magnetic field, the resistivity parallel to the current direction, $\rho_{||}$, will be compared to literature. Perpendicular resistivity, $\rho_{\perp}$, is less well defined than $\rho_{||}$, due to the fast switching of magnetisation direction of the cobalt channel as seen from the sharp downward peaks of the figures above.[21]

For a) $\rho_{||}$ is determined to be $(26.75 \pm 0.27_{\text{Random}} \pm 0.71_{\text{systematic}})\mu\Omega m$ for detailed analysis of the random and systematic errors quoted please see the discussion of errors later on. When measuring the resistance between T1 and T2 a quasi 4 terminal measurement technique was used so the calculated value of resistivity is overestimated. An additional resistance on the order of 1Ω from the gold contacts is included in the measured resistance; the resistance of the cobalt channel is therefore an overestimation.

Resistivity measured for a cobalt film of 30nm in thickness fabricated with the same method of evaporation as used in this experiment gave a value of $13.1\mu\Omega m$.[22] This value is consistent with our measured resistivity value. DeVries et al[22] deposited cobalt films at 295K onto silicon wafers with a 0.4μm SiO_2 layer just as done here in this sample. They claim that grain boundary scattering is the dominant mechanism that determines the resistivity of the thin films with low thicknesses. Grain boundaries in the deposited cobalt films used in this experiment may differ in size compared to the grain boundaries in DeVries which would give a higher value of measured resistivity.[22] Due to the gold contacts being placed on top of the cobalt channel the resistances measured are a sum of the resistance of the gold contacts and the cobalt channel and therefore are slight overestimations.

Another paper that follows a similar fabrication method but tests cobalt films with larger thicknesses, Avery, A. D. et al, report a resistivity of $22.5\mu\Omega m$[2] for a 75nm film at 300K which, again, is consistent with the resistivity reported between T1-T2 and T2-T3. Measured resistivities from this paper will differ slightly from those reported here due to differing contact materials used. Avery, et al used 200nm thick molybdenum contacts whereas 40nm of gold and 3nm of chromium were used as contacts for the experiments presented in this paper. Molybdenum has a resistivity of $10\mu\Omega m$ at 200nm thickness [23] compared to $28\mu\Omega m$ [15] than that of 40mn of gold and so the resistivity measured by Avery, et al will be less than measured here, which it is.

AMR

To quantify the AMR effect the difference in resistance of the channel when magnetisation is saturated parallel and perpendicular to the current direction is needed. When the magnetic field varies perpendicular to the current direction, the magnetisation direction switches very quickly from parallel to the current to perpendicular and then back to parallel. This is due to the fact that the magnetisation is being saturated along the easy axis. Trace and retrace data obtained during these measurements are not the same but are near mirror images of one another through the zero magnetic field axis. This is a tell tale sign of hysteresis in the ferromagnetic cobalt channel and shows a coercivity of around $10mT$.

The AMR measured (using the selective averages) between T1-T2 was 0.42% for trace and 0.36% retrace, for T2-T3, 0.28% for trace and 0.37% for retrace were measured. These results closely agree with the work by Woosik et al[4] who find the %AMR in a 20nm thin cobalt film fabricated in a similar way to be of order 0.4%. Böhnert et al[5] are another group that measured AMR in thin films on SiO_2 substrates but they did not use pure cobalt. Instead, they used a variety of different compositions of cobalt and nickel. They report that the %AMR measured decreases as cobalt content of the thin films increases. Extrapolating from their data a %AMR of less than 1% is expected for a pure cobalt thin film of thickness around 140nm which is consistent with the measured value here.

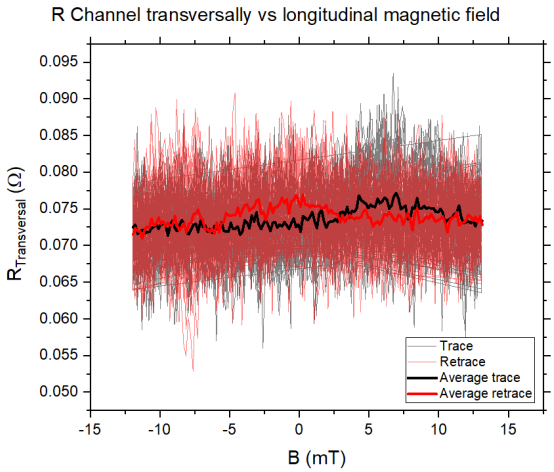

Figure 12: Resistance calculated from the potential difference measured across the channel against the magnetic field applied parallel to the injected current direction in the channel.

Using the hall probes attached to the device, the potential drop across the channel was measured. This voltage should be zero by Ohm's law ($V = IR$) since no current is being injected across the channel. There is, in fact, a very small voltage measured between these two probes indicating that there is a flow of charge between them. As stated before, no current flows directly from one probe to the other perpendicular to the injected current direction, instead, this potential difference is due to a misalignment between the contacts. Assuming a constant resistivity of the channel in all directions, the resistance value measured indicates a misalignment of order 20nm. This misalignment can be attributed to the imperfection of the fabrication process. Gold contacts are made up of grains of order 10nm and this measurement indicates that there is a misalignment of approximately two grain widths between the opposite contacts. No greater precision than this can reliably be obtained with the available fabrication system. Another reason for this slight misalignment may be due to the contact not being in perfect contact with the channel. Later experiments gave poor and unreliable measurements with these hall contacts and one of them became completely unattached and was found to be open circuit.

As with the previous set of measurement data, the raw data was separated into traces and retraces then averaged over to give the bold black and red lines shown in figure 12. The magnitude and shape of the variation in resistance measured is different to that seen in figure 11 a) and b). This variation, therefore, cannot be attributed to AMR and instead it is in fact due to inhomogeneities in the 3nm gold capping layer deposited on the surface of the cobalt channel. Equipotential lines in the gold may be affected by an inhomogeneous capping layer and charges that would typically flow in the direction of injection could, instead, accumulate at the hall contacts causing a small potential difference to arise between the hall probes. Hysteresis can be seen in the measurement with trace and retraces being symmetric and having a coercivity of order $7mT$.

Transversally varying magnetic field

After disassembling the apparatus, rotating the device 90^{o} anticlockwise and remounting it, the magnetic field was swept once again. Now the field increases in the direction of the hard axis causing a slower rotation of the magnetisation vector. At high field the magnetisation vector pointed in the hard axis direction, e.g. perpendicular to injected current flow.

Resistivity of the channel

Figure 13 shows the resistivity profile obtained when varying the applied magnetic field perpendicular to the injected current direction. The peak in resistivity at zero field indicated high resistance when the magnetisation was parallel with the current direction. Hysteresis can be seen by the different peak locations for both trace and retrace curves and coercivity is seen to be around $10mT$. This indicates that only a very small amount of magnetic domains remain magnetised in the hard axis direction after saturation at high field. Comparing figure 13 a) with figure 12 a) from the longitudinally varied magnetic field, the two resistivities measured are consistent with one another, both are of order $26.7\mu\Omega m$. Resistivity of the channel between T2-T3 is also consistent and again is around $3\mu\Omega m$ less than that of the resistivity between T1-T2 due to the quasi-4 terminal nature of the T1-T2 measurement increasing measured resistance by 1Ω from the gold contacts.

At high magnetic field the response seen no longer follows the response expected from AMR but follows the response expected from magnon magnetic scattering [4]. Due to this scattering the perpendicular resistivity state is ill defined. It is possible to extrapolate this value by fitting a linear plot to either side of the peak. The intersection point (at zero applied field) of these two lines was then taken to be the parallel resistivity state.

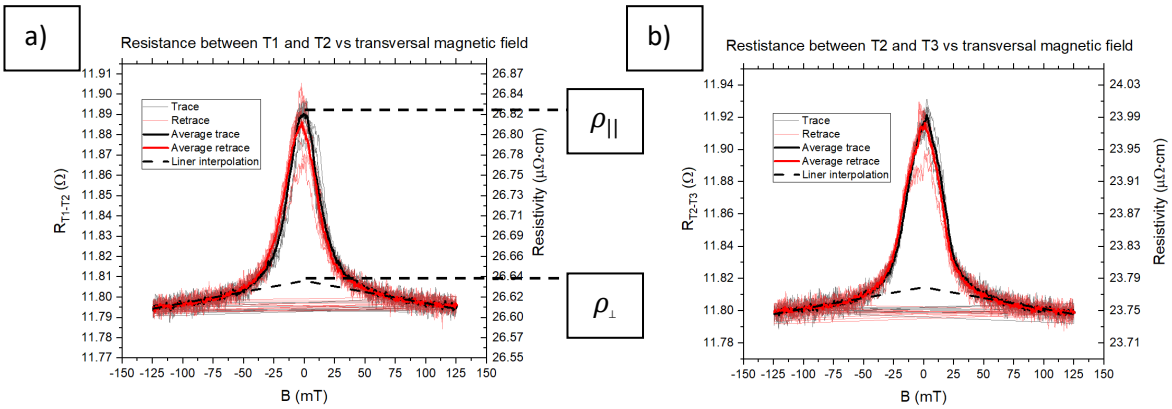

Figure 13: Resistance between a) thermometers 1 and 2 and b) thermometers 2 and 3 for transversally varying magnetic field.

AMR

AMR measured in the transversal orientation in the channel between T1-T2 gave values of 0.68% for the trace curves and 0.64% for retraces. These values are consistent with the AMR measured between T1-T2 in the longitudinal orientation, 0.42% (trace) and 0.36% (retrace). Agreeability is found with the AMR measured with Woosik et al[4] in their 20nm cobalt thin film who quote AMR to be 0.4%. Woosik used a similar fabrication method and measure resistivity and AMR on a SiO_2 substrate. AMR between T2-T3 was measured to be 0.87% for the trace and 0.83% for retrace measurements.

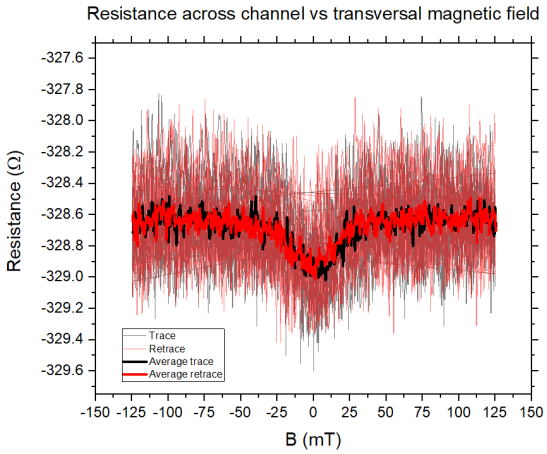

Figure 14: Resistance measurement across the channel for transversally varying magnetic field.

Hall probes were used to measure the resistance of the channel perpendicular to the injected current direction seen in figure 14. Instead of measuring near zero potential difference across the channel, which was expected, the potential difference was both large and negative. This gave calculated resistance values that were wholly inaccurate and not representative of the actual resistance across the cobalt channel. Here it is clear that there is a fault with either of the two hall contacts. These two contacts were only used for the longitudinal thermal measurement across the channel and after that were not used in any further experiments. The data presented in figure 14 will therefore be disregarded.

Summary of results

Electrical contacts placed on top of the channel were used to inject a known current along the length of the channel. The potential differences between thermometers T1 and T2 and also between T2 and T3 were measured. These potential differences were then used, along with Ohm's Law to calculate the resistance of the cobalt channel. Dimensions of the channel, summarised in the appendix, determined through optical images and AFM data were then used to calculate the resistivity. An external magnetic field was varied both parallel and perpendicular to this current direction and the resistivity was measured and the relationship between resistivity and applied magnetic field was recorded. This effect was then quantified by taking the ratio of the resistivity when magnetisation of the channel was saturated along the easy axis and along the hard axis. Resistivities measured between both T1-T2 and T2-T3 for both the longitudinal and transversal magnetic fields were consistent with one another. Recorded resistivities are also consistent with results published by different research groups in similarly fabricated cobalt thin films. [2], [22]

AMR was measured for both the longitudinal and transversal directions and the size of this effect is consistent with previously published AMR results for similar films.[4], [5] Due to failures in fabrication, it was not possible to investigate the differences in AMR or resistivity of the cobalt

channel on the hBN substrate and SiO_2. Next semester it may be possible to implement another lithographic stage in which more gold can be deposited on top of existing, but broken, contacts in an effort to create electrical contact. These measurements can then be repeated in the region of cobalt situated on the hBN and the results can then be compared to those found on the reference SiO_2 substrate.

Thermoelectric measurements

The next series of measurements involved a thermal gradient across the length of the cobalt channel. A current supplied to the heater generated a thermal gradient along which related to a known temperature difference between T1-T2 and also between T2-T3 by use of the calibrations earlier. Here, the same voltage probe set up for the AMR andresistivity measurements was used. By linking potential difference and temperature difference to seebeck coefficient, $S = -\frac{\Delta V}{\Delta T}$, the relative seebeck coefficient of the channel to the gold contacts can be determined. An external magnetic field applied parallel and perpendicular to the direction of the thermal gradient and the seebeck coefficient is recorded as it varied.

Seebeck variation-Longitudinal magnetic fiekd

Thermovoltage was measured between T1-T2, T2-T3 and between the hall probes. Figure 15 shows the variation of this seebeck coefficient with the applied longitudinal magnetic field. As with resistivity measurements, the thermopower measurements have both parallel and perpendicular states for when the magnetisation of the channel is parallel or perpendicular to the thermal gradient. Quoted values of thermopower will be the parallel state values.

The applied magnetic field changes the direction of magnetisation of the channel. Magnetisation is saturated along the easy axis at high field and rotates through the hard axis, peaking at around $7.5mT$. Here it can be concluded that the magnetisation direction of the cobalt channel does, in fact, affect the magnitude of S. The seebeck coefficient increases when magnetisation direction points along the hard axis.

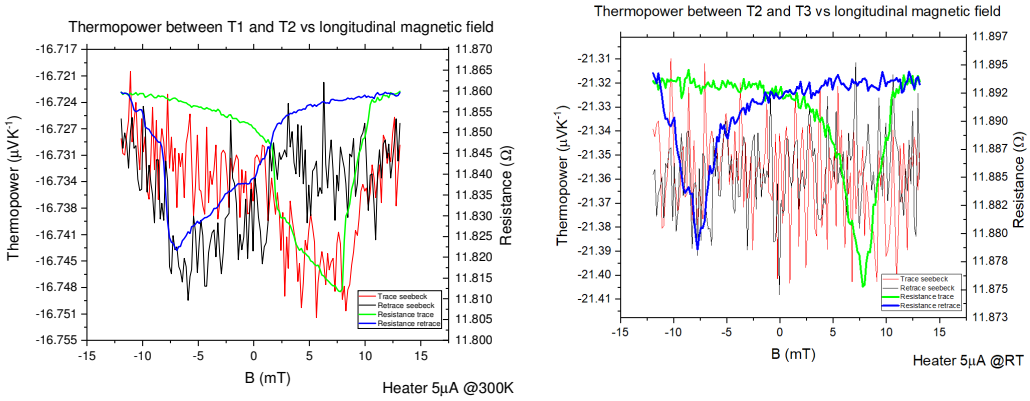

Figure 15: Thermopower (seebeck coefficient) measured between a) thermometers 1 and 2 and b) thermometers 2 and 3 for longitudinally varying magnetic field.

Thermopower in the channel is calculated to be $(-16.7 \pm 3.3_{\text{Random}} \pm 2.1_{\text{systematic}})\mu V/K$ in the parallel state measured between T1 and T2. This value does not agree with the bulk seebeck coefficient quoted in literature of $-25.8\mu V/K$[14] which is expected because, from the mott relation, the thermopower is dependent on the dimensions of the channel through its resistivity. Resistivity increases as thickness of the film decreases [15] so the thermopower is expected to decrease. Other research groups have tested the thermopower in thin cobalt films similar to this one. Avery et al report

a thermopower of -15μV/K for a cobalt film of thickness 75nm[2], [24]. Avery et al used a similar heater arrangement to the one used here, created with a similar lithographic process but made out of molybdenum. The width of the heater is of a similar width to the channel. This may have caused uneven heating in the channel and an inhomogeneous thermal profile to be present in the channel. As such the reported value from Avery et al could be underestimated in magnitude. Avery et al use a thermal isolation platform made out of silicon nitride to keep the cobalt film suspended above the bulk silicon wafer. This reduces loss of heat to the silicon and so will create a different thermal profile in the cobalt film to the one used in these experiments. Thermopower measured here is therefore consistent with the value measured in our experiment but it cannot be directly compared to it.

Resistivity measurements have been overlaid in figure 15 a) and b) to compare the thermopower and AMR profiles. The variation seen in the seebeck coefficient can be quantified with a dimensionless quantity called the magneto-thermoelectric power (MTEP) which is defined as the percentage difference in seebeck coefficient measured in the parallel and perpendicular states. $MTEP = \frac{S-S_{||}}{S_{||}}$. Here, S is the measured seebeck coefficient at a given applied magnetic field and $S_{||}$ is the seebeck coefficient measured when magnetisation in the channel is saturated parallel to the thermal gradient. MTEP is maximum when $S = S_{\perp}$, e.g. the magnetisation of the channel is perpendicular to the thermal gradient, this corresponds to high applied magnetic field. The thermopower profile closely follows that of the AMR seen in the channel which shows that these two effects are related. The size of the seebeck deviation however is much smaller than that of AMR, a change of only 0.1% is recorded between parallel and perpendicular states as measured between T1-T2. AMR, in contrast, was 0.4% in this region. Böhnert et al[5] measured MTEP in thin films of thickness 140nm with different compositions of cobalt and nickel. They find a large non linear decrease in observed MTEP with cobalt content. Less than 1% MTEP is expected for a pure cobalt film which is consistent with measured values here.

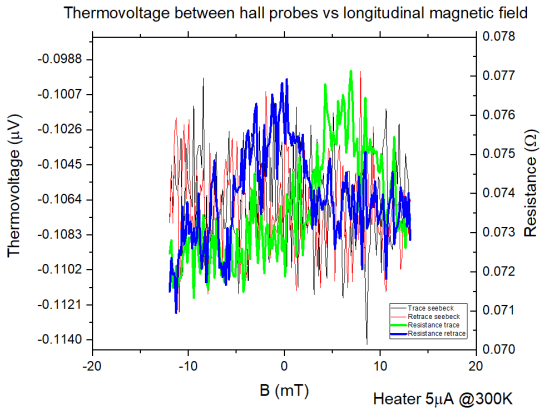

Figure 16: Thermalvoltage measured between the hall probes vs longitudinal magnetic field.

Assuming that the seebeck coefficient, calculated from the thermometry measurements previously, is constant across the width of the channel the temperature difference across the channel can be estimated, figure 16 shows the thermovoltage measured across the channel. This temperature difference is estimated to be $6mK$, which is a 1.4% of the temperature difference between consecutive thermometers. This temperature difference can be attributed to the inhomogeneity in the thermal profile across the width of the channel. In the real world it is very difficult to create a perfectly homogeneous thermal profile since exact symmetry and consistency is required. This device was made to be as symmetric as possible but it is far from perfect. The fabrication process causes misalignments, uses finite sized grains to make up the channel and uses a non perfect electron

lithography procedure, all of which contribute to imperfections in the device. Therefore it is not surprising to see a slight temperature difference across the width of the channel.

Seebeck variation-Transversal magnetic field

After longitudinal measurements were complete, the device was un-mounted and re-mounted after a 90° anticlockwise rotation. Firstly it can be seen in figure 17 that there is a transversal thermopower response. This transversal response is better defined than the longitudinal due to the magnetisation of the channel being forced along the hard axis which causes ***M*** to be rotated slower. A thermopower of -16.8$\mu V/K$ is measured for the parallel orientation between T1 and T2. This value is consistent with the measured seebeck coefficient from the longitudinally varying magnetic field measurements. Again, this agrees with Avery et al[2] and the MTEP was measured to be 0.1%, consistent with Böhnert et al[5].

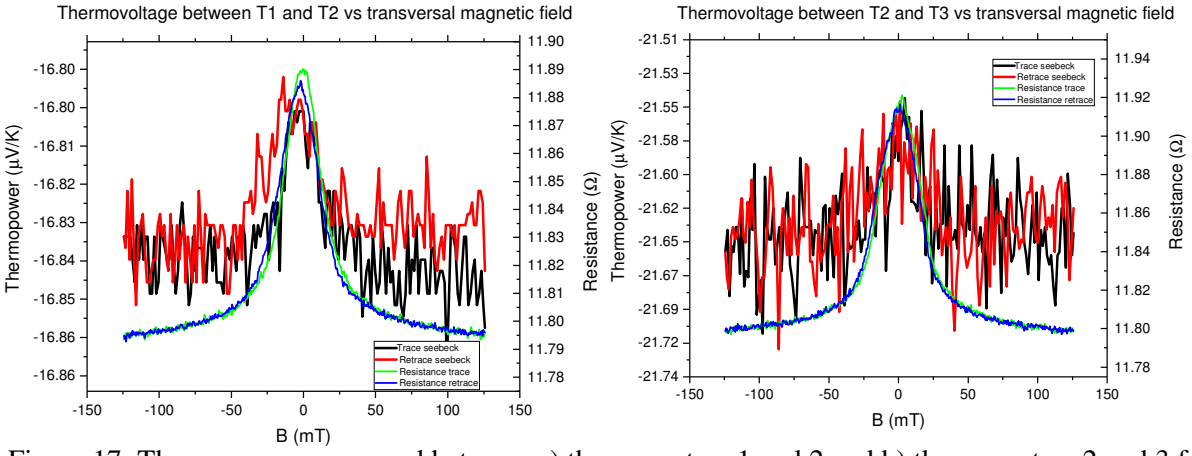

Figure 17: Thermopower measured between a) thermometers 1 and 2 and b) thermometers 2 and 3 for transversally varying magnetic field.

Magnetothermoelectric response of contacts

One large assumption that has been used throughout all of the thermoelectric measurements and analysis is that the temperature difference, ΔT, between consecutive thermometers is constant. This is assumed since there the heater is applied with a constant current; this created an assumed constant and homogeneous thermal profile throughout the channel. Specific design considerations were put in place, such as a very wide heater to channel width ratio, to limit any discontinuities. To test if this assumption held, the four point resistance of the thermometers was measured while the applied magnetic field was swept and the heater was first, off and then on. The thermometer and cobalt channel are in contact with one another. The electrical arrangement here can be thought of as two resistors in a parallel configuration. Typically, the gold thermometer has a much lower resistance than the cobalt channel due to its low resistivity compared to cobalt. The four point resistance measured, therefore, it the resistance of the whole arrangement of the thermometer and part of the cobalt channel. If the resistance of the channel changes then the measured four point resistance will also change. Measured resistance can be seen in figure 18.

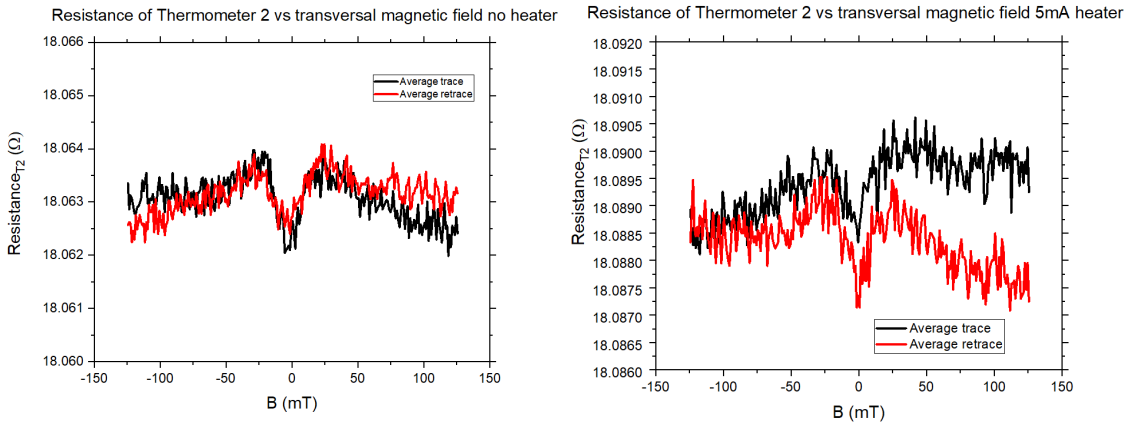

Figure 18 shows the 4 point resistance of thermometer 2 against the applied magnetic field strength while in the transversal direction for a) zero applied heater current and b) 5*mA* heater current.

As the magnitude of the applied field increases, the measured resistance also increases and then decreases linearly at high applied filed. The initial increase is due to the resistance of the cobalt channel increasing as the magnetisation direction of the channel is oriented along the easy axis. A high channel resistance causes the overall measured resistance to increase. The slow linear decrease in measured resistance is due to magnon magnetic scattering[4], this is the same effect that caused the linear decrease in resistance see in the transversal AMR measurements. Since the same variation in resistance is visible in both measurements, when the heater is supplied with no current and 5*mA*, it can be concluded that the addition of a thermal gradient does not affect the resistance of the thermometers to a large degree. As the variation seen is around 0.01% of the measured resistance, the effect can be ignored during error analysis and the assumption of a constant temperature gradient holds.

Error estimation

Parameter	Value	Raw error	Percentage error	Source of error
R_s	1.000 MΩ	0.003 MΩ	0.30 %	Measured from series resistor
V_s	5.000 V	0.001 V	0.02 %	Lock-in amplifier, quoted from manual
Thickness of cobalt	33 nm	0.53 nm	1.61 %	From AFM imagery and surface roughness
Width of cobalt	2.14μm	0.03μm	1.59 %	From optical imagery
Length of cobalt	3.14μm	0.04μm	1.41%	From optical imagery
ΔT	0.413K	0.05K	12.7%	From thermal calibration

Table 1: Summary of error estimated used for calculations concerning thermometers 1 and 2.

Errors, for resistivity for example, were calculated in quadrature: $\frac{\delta\rho}{\rho} = \sqrt{\left(\frac{\delta R}{R}\right)^2 + \left(\frac{\delta w}{w}\right)^2 + \left(\frac{\delta t}{t}\right)^2 + \left(\frac{\delta l}{l}\right)^2}$ where $\frac{\delta R}{R} = \frac{1}{10}\sqrt{\left(\frac{\delta V}{V}\right)^2 + \left(\frac{\delta V_S}{V_S}\right)^2 + \left(\frac{\delta R_S}{R_S}\right)^2}$. These equations come from the formula for resistivity $\rho = \frac{V}{10I}\frac{wt}{l}$ where I=Vs/Rs is the current injected into the channel through a $1M\Omega$ series resistor from the lock in amplifier at voltage V_s, V is the measured potential

difference between two contacts and w, t and l are the width, thickness and length of the channel between those contacts. The thickness of the channel is the largest source of uncertainty. Random noise in the measurements are quoted for each individual measurement calculated from the raw data or fit parameters. For thermal measurements, the very large uncertainty in the temperature difference ΔT was the dominant source of error. All errors quoted in table 1 are for thermometer 1 to thermometer 2.

Conclusion

In an energy conscious world it is important to investigate new ways of creating more efficient technology. A new technology that is looking very promising for the advancement of computing technology is spintronics. Magnetised ferromagnetic thin films, such as cobalt, are particularly useful in the realisation of new spintronic devices.[3], [25], [26] As such, researching how heat and charge flow through these films is important to the understanding and development of this technology. The aim of this semester's project was to measure and compare the anisotropic magnetoresistance and magnetothermoelectric responses of a 30nm thick cobalt film on SiO_2 and hBN substrates. Due to faults in the fabrication process it was not possible to achieve this outcome.

A device was designed from scratch to specifically measure electrical and thermal properties of a cobalt thin film on a thin flake of hBN situated on a SiO_2 substrate. After designing and iterating the device, a group of PhD students helped to fabricate the device by use of electron beam lithography. Next the device was mounted in a cryostat and each of the contacts was electrically connected to a breakout box that allowed lock in amplifiers to be attached to the contacts. Electrical charge was injected into the cobalt channel by use of the gold contacts. Potential difference measurements were then taken between different contacts to estimate the properties of the cobalt channel itself. Four point electrical measurements were used when possible to eliminate as much contact resistance contribution as possible. Interfacial resistance is still present between the cobalt and gold so measured results are slightly overestimated.

On SiO_2, the resistivity of the cobalt channel was determined to be $(26.75 \pm 0.27_{\text{Random}} \pm 0.71_{\text{systematic}})\mu\Omega m$ which is consistent with other thin films that followed similar fabrication methods are of similar thicknesses. AMR was determined to be 0.4% which is also consistent with literature.[2]Next semester the AMR on hBN will be measured and compared with that on the reference SiO_2 substrate. A difference is expected since the cobalt may grow differently on the atomically flat hBN flake. Next the thermopower of the channel was measured. This was done by applying a known current into the heater and thus creating a known temperature difference between consecutive thermometers. The voltage between these two thermometers was measured and the seebeck relation was used to determine the thermopower (seebeck coeffiecient). An external magnetic field was applied and swept to change the direction of the magnetisation of the cobalt channel to being along the easy or hard axes. This caused a variation in the measured thermopower quantified by the MTEP. The measured thermopower was found to be $(-16.7 \pm 3.3_{\text{Random}} \pm 2.1_{\text{systematic}})\mu V/K$ and MTEP are both consistent with literature on the SiO_2 substrate.

Since the device was broken during fabrication, a new experiment was performed in which the four point resistance of the thermometers was measured while the heat was on and off and the magnetisation of the channel was rotated. If a large difference in measured resistance was seen when the heater was on as opposed to off then the assumption that the temperature difference between consecutive contacts is constant would no longer hold. Since resistances measured with the heater on

and off were consistent with one another, the assumption was shown to hold to a certain extent. The Variation in individual resistance measurements with the magnetic field can be attributed to current flowing though the gold contacts leaking into the cobalt channel and experiencing AMR then returning back into the gold contact. This effect extremely small and as such is negligible in the quoted values of resistivity, AMR, thermopower and MTEP.

Further study

Due to there being no working thermometers on the hBN substrate, it is important to either fabricate a new device entirely or attempt to repair the current one. Repairing will be tried first as it will be simple and quick. All that is needed to be done is to perform another lift off process and deposit more gold on top of the contacts that are broken to make sure there is electrical contact. There may be some slight issues with repairing the broken heater as the broken cobalt anchor destroyed the upper half of it. Attempts will be made to salvage and repair as much of the original design as possible and to achieve the intended goal of comparing AMR and magnetothermoelectric properties on the hBN substrate to the SiO_2 reference.

Next semester, steps can be taken to measure the temperature dependence of the properties measured in this paper. Liquid helium can be used to decrease the device's temperature down to a few Kelvin, therefore eliminating much phonon activity in the channel. Temperature dependence of the magnetothrmopower and anisotropic magnetoresistance can also be measured on and off the hBN substrate and compared. This dependence has not been measured before for thin cobalt films on hBN.

References

[1] L. E. Bell, "Cooling, Heating, Generating Power, and Recovering Waste Heat with Thermoelectric Systems," *Science (80-.).*, vol. 321, no. 5895, p. 1457 LP-1461, Sep. 2008.

[2] A. D. Avery, R. Sultan, D. Bassett, D. Wei, and B. L. Zink, "Thermopower and resistivity in ferromagnetic thin films near room temperature," *Phys. Rev. B - Condens. Matter Mater. Phys.*, vol. 83, no. 10, pp. 1–4, 2011.

[3] A. Hoffmann and S. D. Bader, "Opportunities at the frontiers of spintronics," *Phys. Rev. Appl.*, vol. 4, no. 4, pp. 1–18, 2015.

[4] W. Gil, D. Görlitz, M. Horisberger, and J. Kötzler, "Magnetoresistance anisotropy of polycrystalline cobalt films: Geometrical-size and domain effects," *Phys. Rev. B - Condens. Matter Mater. Phys.*, vol. 72, no. 13, pp. 1–10, 2005.

[5] T. Böhnert, V. Vega, A. K. Michel, V. M. Prida, and K. Nielsch, "Magneto-thermopower and magnetoresistance of single Co-Ni alloy nanowires," *Appl. Phys. Lett.*, vol. 103, no. 9, pp. 0–5, 2013.

[6] T. R. Mcguire and R. I. Potter, "Anisotropic Magnetoresistance in Ferromagnetic 3D Alloys," *IEEE Trans. Magn.*, vol. 11, no. 4, pp. 1018–1038, 1975.

[7] D. K. C. MacDonald, *Thermoelectricity: An Introduction to the Principles.* Dover Publications, 2006.

[8] T. McGuire and R. Potter, “Anisotropic magnetoresistance in ferromagnetic 3d alloys,” *IEEE Trans. Magn.*, vol. 11, no. 4, pp. 1018–1038, Jul. 1975.

[9] E. De Ranieri *et al.*, “Lithographically and electrically controlled strain effects on anisotropic magnetoresistance in (Ga,Mn)As,” vol. 3, pp. 1–11, 2018.

[10] F. A. Rohrman, “The Theory of the Properties of Metals and Alloys (Mott, N. F.; Jones, H.),” *J. Chem. Educ.*, vol. 14, no. 2, p. 99, Feb. 1937.

[11] Ch. Hollauer, “Modeling of Thermal Oxidation and Stress Effects.” [Online]. Available: http://www.iue.tuwien.ac.at/phd/hollauer/node7.html. [Accessed: 20-Dec-2018].

[12] L. H. Li and Y. Chen, “Atomically Thin Boron Nitride: Unique Properties and Applications,” *Adv. Funct. Mater.*, vol. 26, no. 16, pp. 2594–2608, 2016.

[13] J. W. C. De Vries, “Temperature and thickness dependence of the resistivity of thin polycrystalline aluminium, cobalt, nickel, palladium, silver and gold films,” *Thin Solid Films*, vol. 167, no. 1–2, pp. 25–32, 1988.

[14] M. J. Laubitz and T. Matsumura, “Transport Properties of the Ferromagnetic Metals. I. Cobalt,” *Can. J. Phys.*, vol. 51, no. 12, pp. 1247–1256, Jun. 1973.

[15] T. H. Gilani and D. Rabchuk, “Electrical resistivity of gold thin film as a function of film thickness,” *Can. J. Phys.*, vol. 96, no. 3, pp. 272–274, 2018.

[16] K. S. Novoselov and A. K. Geim, “Electric Field Effect in Atomically Thin Carbon Films,” *Science (80-.).*, vol. 306, no. October, pp. 666–670, 2004.

[17] I. J. Vera-Marun, J. J. Van Den Berg, F. K. Dejene, and B. J. Van Wees, “Direct electronic measurement of Peltier cooling and heating in graphene,” *Nat. Commun.*, vol. 7, no. May, pp. 1–6, 2016.

[18] J. T. Perkins, “Perkins , Jason T . Electron-Beam Lift-off Lithography for Fabrication of Patterned Sapphire ... May 2006,” 2006.

[19] J. H. Scofield, “Frequency-domain description of a lock-in amplifier,” *Am. J. Phys.*, vol. 62, no. 2, pp. 129–133, 1994.

[20] A. S. . Alenitsyn, Alexander G.; Butikov, Eugene I.; Kondraryez, *Concise Handbook of Mathematics and Physics.* CRC Press, 1997.

[21] X. K. Hu *et al.*, “Magnetothermoelectric figure of merit of Co/Cu multilayers,” *Appl. Phys. Lett.*, vol. 104, no. 9, 2014.

[22] J. W. C. Devries, “TEMPERATURE AND THICKNESS DEPENDENCE OF THE RESISTIVITY OF THIN POLYCRYSTALLINE ALUMINIUM, COBALT, NICKEL, PALLADIUM, SILVER AND GOLD FILMS,” vol. 167, pp. 25–32, 1988.

[23] A. M. Hofer, J. Schlacher, J. Keckes, J. Winkler, and C. Mitterer, “Sputtered molybdenum films: Structure and property evolution with film thickness,” *Vacuum*, vol. 99, pp. 149–152, 2014.

[24] R. Sultan, A. D. Avery, G. Stiehl, and B. L. Zink, “Thermal conductivity of micromachined low-stress silicon-nitride beams from 77 to 325 K,” *J. Appl. Phys.*, vol. 105, no. 4, 2009.

[25] A. W. Cummings, S. O. Valenzuela, F. Ortmann, and S. Roche, “Graphene spintronics,” *2D Mater. Prop. Devices*, vol. 9, no. October, pp. 197–218, 2017.

[26] P. Seneor, B. Dlubak, M. B. Martin, A. Anane, H. Jaffres, and A. Fert, "Spintronics with graphene," *MRS Bull.*, vol. 37, no. 12, pp. 1245–1254, 2012.

Health and safety risk assessment

Date:	**Assessed by:**	**Location:**
30/09/2018	**Ben Snow**	**Lab room B.008** **Schuster building**

Task / premises:

Loading and unloading a spintronic device into a cryostat and attaching a vacuum pump and other electrical equipment and the associated measurements of such a device. Use of cryogenic liquid helium.

Activity	**Hazard**	**Who might be harmed and how?**	**Existing measures to control risk**	**Risk rating**
Extended use of computers	Poor working environment	User. Fatigue, stress, muscular or skeletal injury, headaches, eye strain	• Adequate lighting of computer area • No obstructions under desk • Good posture promoting chairs • University support for stress and counselling • Taking frequent breaks and getting fresh air	Medium
Use of electrical laboratory equipment	Electricity, stray wires	User. Electrical shock, burns, fire, tripping over loose wires	• Users are trained and informed how to use equipment before use • All electrical equipment are annually PAT tested and out of date or failed equipment are not to be used • Obvious sparks or damages are reported immediately to lab staff • Grounding bracelets are used when operating electrical equipment • Grounding of electrical equipment • Cable tidy's to keep workspace clear	Medium
Use of pressure valve and lids of liquid helium containers	Dewar exploding	Anyone in the lab	• Pressure must not exceed limit stated on Dewar • Use of safety valve on the dewar that releases excess pressure build up • Specialised connector to dewar that only allows inlet to be connected • Disconnect the decanting line slowly to avoid squirting of liquid helium	Medium

Activity	Hazard	Who might be harmed and how?	Existing measures to control risk	Risk rating
Dispending of cryogenic liquid	Leaks and spills leading to asphyxiation, cold burns from contact with liquid	User and anyone in the lab	• Only those with adequate training are allowed to perform this procedure • Oxygen depletion monitors are kept in the areas near to dewars • Make sure pressure valve is sealed before dispensing liquid • Signs are displayed near liquid helium containers • Cryogenic gloves to be worn to protect from spills • Stand behind the dewar when dispensing takes place • Storage of dewars in well ventilated areas to reduce impact of spillage	Medium
Formation of ice on dewar	Explosion of dewar and ejection of ice at high speed	User and anyone in the lab	• Ice blockages may form inside the dewar neck if moisture comes into contact with the cold gas. This may prevent proper ventilation and unwanted pressure build-up in the dewar • Dewars are fit with protective caps and are checked before use • Never leave dewars uncapped and ensure dewars are empty after use • If an ice plug forms immediately evacuate and alert the School Safety Advisor.	High
Touching cold pipes and surfaces	Cold pipes, exposed cold materials and surfaces	User	• Don't touch cold surfaces and make sure that cryogenic gloves are worn at all times • Burns may take time to manifest after and exposure so call a first aider if there is any doubt about a possible burn	Medium
Breathing in cold fumes and vapour	Mist and fumes from liquid helium	User	• Never consume cryogenic liquid as serious damage can be inflicted to the lungs, mouth and throat. Gas occupies a must greater volume than the liquid so ingesting even a small amount will cause long term, possibly fatal damage	High
Trapping of cryogenic liquid in clothing	Trapped liquid helium in clothing	User	• Always ensure appropriate PPE is worn (cryogenic gloves, aprons etc) • Avoid wearing clothes with pockets or folds that could trap and collect spilt liquid • Never wear shorts or skirts while using cryogenic liquids • Closed toe footwear to be used, absolutely no sandals, flip flops, open toed shoes or shoes not covering up to at least the ankle should be worn • Trousers must fit over top of shoes	Medium
Spillage of cryogenic liquid	Damaged floor and nearby equipment	User and anyone in the lab	• Spilt cryogenic liquid can cause materials and the floor to become brittle and collapse under exposure • Report any spillages to the School Safety advisor immediately and evacuate the building	Low
Use of vacuum pump	Breakage of glass under vacuum	User and anyone in the lab	• Visual check for broken glass before turning on vacuum pump	Low

Activity	Hazard	Who might be harmed and how?	Existing measures to control risk	Risk rating
Use if vacuum pump	Electricity and electric shock	User	• Normal precautions followed when using electrical equipment • Electrical equipment is routinely PAT tested and only equipment that passes these tests are used • Obvious hazards (open wires, sparks etc) are reported to technical staff and removed from the lab	Low
Storing items at height	Objects falling, lifting objects above head height, broken glass or plastic	Anyone in the lab close to the stored items Bodily injuries including cuts or head injuries. Damage to equipment. Contact with harmful substances	• Avoid storing items at height • No storage of hazardous chemicals or substances above head height • No storage of heavy or large items at height • Boxes stored at height must be closed to limit falling of contained items • No glass stored at height	Low
Lone working	No one around to help if an accident occurs or there is an emergency	User	• No lone working allowed in the laboratory under any circumstances	High

Appendix

Origin script used to split trace and retrace data and to perform averages over both:

```
Range Xref = 1;
int Xsize = Xref.GetSize();

int counter_tr = 1;
int counter_re = 1;

int n_decimals = 3;
int n_tr = 0;
int n_re = 0;

int nColXref = 1;
int nColX1 = 12;
int nColY1 = 15;

int ii=1, jj=1;

//create columns
wks.addcol();
wks.addcol();
wks.addcol();
wks.addcol();

int nColYre = wks.ncols;
```

```
int nColXtr = nColYre-3;
int nColYtr = nColYre-2;
int nColXre = nColYre-1;

wcol(nColXtr)[L]$ = "B-trace";
wcol(nColYtr)[L]$ = "V3-trace";
wcol(nColXre)[L]$ = "B-retrace";
wcol(nColYre)[L]$ = "V3-retrace";

wcol(nColXtr)[U]$ = "T";
wcol(nColYtr)[U]$ = "V";
wcol(nColXre)[U]$ = "T";
wcol(nColYre)[U]$ = "V";

wks.col$(nColXtr).type = 4;
wks.col$(nColYtr).type = 1;
wks.col$(nColXre).type = 4;
wks.col$(nColYre).type = 1;

for (ii = 1; ii <= Xsize; ii++)
{

if (ii == 1)
{
   if (wcol(nColXref)[1] < 0)
   {
      wcol(nColXtr)[1] = wcol(nColX1)[1];
      wcol(nColYtr)[1] = wcol(nColY1)[1];
      counter_tr = counter_tr + 1;
      n_tr = 1;
   }
   if (wcol(nColXref)[1] > 0)
   {
      wcol(nColXre)[1] = wcol(nColX1)[1];
      wcol(nColYre)[1] = wcol(nColY1)[1];
      counter_re = counter_re + 1;
      n_re = 1;
   }
}
else if (round((wcol(nColXref)[ii]),n_decimals) == round((wcol(nColXref)[ii-1]),n_decimals))
{
   if (round((wcol(nColXref)[ii+1]),n_decimals) > round((wcol(nColXref)[ii]),n_decimals))
   {
      wcol(nColXtr)[counter_tr] = wcol(nColX1)[ii];
      wcol(nColYtr)[counter_tr] = wcol(nColY1)[ii];
      counter_tr = counter_tr + 1;
      n_tr += 1;
   }
   else
   {
      wcol(nColXre)[counter_re] = wcol(nColX1)[ii];
      wcol(nColYre)[counter_re] = wcol(nColY1)[ii];
      counter_re = counter_re + 1;
      n_re += 1;
   }
}
else if (round((wcol(nColXref)[ii]),n_decimals) > round((wcol(nColXref)[ii-1]),n_decimals))
{
   wcol(nColXtr)[counter_tr] = wcol(nColX1)[ii];
   wcol(nColYtr)[counter_tr] = wcol(nColY1)[ii];
   counter_tr = counter_tr + 1;
}
else if (round((wcol(nColXref)[ii]),n_decimals) < round((wcol(nColXref)[ii-1]),n_decimals))
{
   wcol(nColXre)[counter_re] = wcol(nColX1)[ii];
   wcol(nColYre)[counter_re] = wcol(nColY1)[ii];
   counter_re = counter_re + 1;
}
}


int nPoints = Xsize/(n_tr + n_re);
double xsum = 0;
double ysum = 0;

//create columns for average
wks.addcol();
wks.addcol();
wks.addcol();
wks.addcol();

int nColYreavg = wks.ncols;
int nColXtravg = nColYreavg-3;
int nColYtravg = nColYreavg-2;
int nColXreavg = nColYreavg-1;
```

```
wcol(nColXtravg)[L]$ = "Bavg-trace";
wcol(nColYtravg)[L]$ = "V3avg-trace";
wcol(nColXreavg)[L]$ = "Bavg-retrace";
wcol(nColYreavg)[L]$ = "V3avg-retrace";

wcol(nColXtravg)[U]$ = "T";
wcol(nColYtravg)[U]$ = "V";
wcol(nColXreavg)[U]$ = "T";
wcol(nColYreavg)[U]$ = "V";

wks.col$(nColXtravg).type = 4;
wks.col$(nColYtravg).type = 1;
wks.col$(nColXreavg).type = 4;
wks.col$(nColYreavg).type = 1;

for (ii = 1; ii <= nPoints; ii++)
{
   xsum = 0;
   ysum = 0;
   for (jj = 1; jj <= n_tr; jj++)
   {
      xsum = xsum + wcol(nColXtr)[(jj-1)*nPoints + ii];
      ysum = ysum + wcol(nColYtr)[(jj-1)*nPoints + ii];
   }
   wcol(nColXtravg)[ii] = xsum/n_tr;
   wcol(nColYtravg)[ii] = ysum/n_tr;

   xsum = 0;
   ysum = 0;
   for (jj = 1; jj <= n_re; jj++)
   {
      xsum = xsum + wcol(nColXre)[(jj-1)*nPoints + ii];
      ysum = ysum + wcol(nColYre)[(jj-1)*nPoints + ii];
   }
   wcol(nColXreavg)[ii] = xsum/n_re;
   wcol(nColYreavg)[ii] = ysum/n_re;
}
```